Monthly Notices
of the
ROYAL ASTRONOMICAL SOCIETY

MNRAS **489,** 2478–2487 (2019)
Advance Access publication 2019 August 23

doi:10.1093/mnras/stz2351

WASP-169, WASP-171, WASP-175, and WASP-182: three hot Jupiters and one bloated sub-Saturn mass planet discovered by WASP-South

L. D. Nielsen [1]★ F. Bouchy,[1] O. D. Turner [1] D. R. Anderson [2] K. Barkaoui,[3,4] Z. Benkhaldoun,[4] A. Burdanov,[3] A. Collier Cameron,[5] L. Delrez [3,6] M. Gillon,[3] E. Ducrot,[3] C. Hellier,[2] E. Jehin,[3] M. Lendl [1,7] P. F. L. Maxted,[2] F. Pepe,[1] D. Pollacco,[8,9] F. J. Pozuelos,[3] D. Queloz,[1,6] D. Ségransan,[1] B. Smalley [2] A. H. M. J. Triaud,[10] S. Udry[1] and R. G. West [8,9]

Affiliations are listed at the end of the paper

Accepted 2019 August 12. Received 2019 July 15; in original form 2019 April 23

ABSTRACT

We present the discovery of four new giant planets from the Wide Angle Search for Planets-South (WASP-South), three hot Jupiters and one bloated sub-Saturn mass planet: WASP-169b, WASP-171b, WASP-175b, and WASP-182b. Besides the discovery photometry from WASP-South we use radial velocity measurements from CORALIE and HARPS and follow-up photometry from EulerCam, TRAPPIST-North and -South, and SPECULOOS. WASP-169b is a low-density Jupiter ($M = 0.561 \pm 0.061\ M_{\rm Jup}$, $R = 1.304^{+0.150}_{-0.073}\ R_{\rm Jup}$) orbiting a $V = 12.17$ F8 subgiant in a 5.611 d orbit. WASP-171b is a typical hot Jupiter ($M = 1.084 \pm 0.094\ M_{\rm Jup}$, $R = 0.98^{+0.07}_{-0.04}\ R_{\rm Jup}$, $P = 3.82$ d) around a $V = 13.05$ G0 star. We find a linear drift in the radial velocities of WASP-171 spanning 3.5 yr, indicating the possibility of an additional outer planet or stellar companion. WASP-175b is an inflated hot Jupiter ($M = 0.99 \pm 0.13\ M_{\rm Jup}$, $R = 1.208 \pm 0.081\ R_{\rm Jup}$, $P = 3.07$ d) around a $V = 12.04$ F7 star, which possibly is part of a binary system with a star 7.9 arcsec away. WASP-182b is a bloated sub-Saturn mass planet ($M = 0.148 \pm 0.011\ M_{\rm Jup}$, $R = 0.850 \pm 0.030\ R_{\rm Jup}$) around a metal-rich $V = 11.98$ G5 star ([Fe/H] $= 0.27 \pm 0.11$). With an orbital period of $P = 3.377$ d, it sits right in the apex of the sub-Jovian desert, bordering the upper and lower edge of the desert in both the mass–period and radius–period plane. WASP-169b, WASP-175b, and WASP-182b are promising targets for atmospheric characterization through transmission spectroscopy, with expected transmission signals of 121, 150, and 264 ppm, respectively.

Key words: planets and satellites: detection – planets and satellites: individual: WASP-169b – planets and satellites: individual: WASP-171b – planets and satellites: individual: WASP-175b – planets and satellites: individual: WASP-182b.

1 INTRODUCTION

The Wide Angle Search for Planets (WASP; Pollacco et al. 2006) survey has since first light in 2006 discovered almost 200 transiting, close-in, giant exoplanets. These planets have provided great insight into exoplanetology as they enable studies of bulk properties, mass and radius from the transit photometry, and radial velocity (RV) follow-up. Furthermore, WASP has provided prime targets for in-depth characterization of star–planet interactions, exoplanet atmospheres (Birkby et al. 2013; de Kok et al. 2013), planetary winds (Brogi et al. 2016), and even the RV shift of the planets themselves (Snellen et al. 2010).

Furthermore, WASP and other wide field ground-based surveys have been instrumental in discovering exoplanets bordering the sub-Jovian desert. The desert is constituted by a shortage of intermediate-sized planets (1.0–0.1 $R_{\rm Jup}$) in close-in orbits (period <5 d; Szabó & Kiss 2011; Mazeh, Holczer & Faigler 2016; Fulton & Petigura 2018). This phenomenon is evident when analysing the distribution of periods for exoplanets as a function of both planetary radius and mass, as illustrated in Fig. 10. Ground-based surveys have traditionally targeted planets sitting on the upper edge of the desert, due to detection limits. A notable exception to this rule is NGTS-4b (West et al. 2019), a sub-Neptune-sized planet in a

★ E-mail: louise.nielsen@unige.ch

1.34 d orbit around a K-dwarf. NGTS-4b is situated well within the sub-Jovian desert, challenging current theories of photoevaporation.

Space-based surveys, in particular *Kepler* (Borucki et al. 2010), have provided more targets constraining the lower edge, but mainly in the radius–period plane, as many of these targets are too faint for ground-based follow up. The *Transiting Exoplanet Survey Satellite* (*TESS*; Ricker et al. 2015) is now changing the landscape of exoplanetology providing hundreds of transiting exoplanet candidates around bright stars, most of them appropriate for mass characterization with RVs.

In this study, we present four giant planets discovered with WASP-South: three hot Jupiters and one bloated sub-Saturn mass planet: WASP-169b, WASP-171b, WASP-175b, and WASP-182b, all orbiting relatively bright G- and F-type stars. We perform a global Markov chain Monte Carlo (MCMC) analysis of the discovery data from WASP-South, follow-up photometry from EulerCam, Transiting Planets and Planetesimals Small Telescope (TRAPPIST)-North, TRAPPIST-South, and Search for habitable Planets EClipsing ULtra-cOOl Stars (SPECULOOS) and RVs from CORALIE and High Accuracy Radial Velocity Planet Searcher (HARPS). WASP-169b is a low-density Jupiter ($M = 0.561 \pm 0.061\,M_{\rm Jup}$, $R = 1.304^{+0.150}_{-0.073}\,R_{\rm Jup}$, $P = 5.611$ d) and WASP-175b ($M = 0.99 \pm 0.13\,M_{\rm Jup}, R = 1.208 \pm 0.081\,R_{\rm Jup}, P = 3.07$ d), making them interesting targets for atmospherics characterization. WASP-171b is a typical hot Jupiter ($M = 1.084 \pm 0.094\,M_{\rm Jup}$, $R = 0.98^{+0.07}_{-0.04}\,R_{\rm Jup}$, $P = 3.82$ d) with a possible additional companion indicated by a linear drift in the RVs. WASP-182b is a bloated sub-Saturn mass planet ($M = 0.148 \pm 0.011\,M_{\rm Jup}$, $R = 0.850 \pm 0.030\,R_{\rm Jup}$, $P = 3.377$ d) sitting in the apex of the sub-Jovian desert, bordering the upper and lower edge of the desert in both the radius–period and mass–period plane.

2 OBSERVATIONS

2.1 Discovery photometry from WASP-South

The host stars of the four planets presented in this paper have been surveyed by WASP-South spanning several years, with WASP-182 being the target monitored for the longest time, dating back to 2006. WASP-South consisted, during the observations reported here, of eight 20 cm individual *f*/1.8 lenses mounted on the same fixture. Each lens was equipped with a 2k × 2k CCD with a plate scale of 13.7 arcsec pixel^{-1}. The wide 7.°8 × 7.°8 field of view, allowed WASP-South to cover 1 per cent of the sky in each pointing, targeting stars with 9–13 mV. The 20 cm lenses have since been replaced with 85 mm lenses, allowing the survey to target planets around brighter stars such WASP-189b (Anderson et al. 2018).

Transit events are searched for in the discovery photometry using the box least-square method as described in Collier Cameron et al. (2006). Targets with transits consistent with a planet-sized object are ranked according to Collier Cameron et al. (2007) and put forward for follow-up observations with a wide range of facilities. Both high-resolution spectroscopy and photometry are used to confirm the planetary nature of the transiting object and ultimately measure both mass and radius precisely as described in the following sections. A summary of the observations used in this study can be found in Table 1.

Table 1. Summary of the discovery photometry, follow-up photometry, and radial velocity (RV) observations of WASP-169, WASP-171, WASP-175, and WASP-182 from all facilities. Note time of meridian flip (MF) for WASP-169 on the TRAPPIST telescopes in BJD (245 0000).

Date	Source	No. obs/filter
WASP-169		
2011 Jan–2012 Apr	WASP-South	24 205
2015 Mar–2017 May	CORALIE	25
2016 Feb 08 MF at 7427.6706	TRAPPIST-South	$I+z$
2018 Jan 04 MF at 8123.5899	TRAPPIST-North	$I+z$
2018 Dec 01 MF at 8454.6814	TRAPPIST-North	z'
2019 Feb 23 MF at 8538.6286	TRAPPIST-South	z'
WASP-171		
2011 Jan–2012 June	WASP-South	77 507
2015 June–2018 Dec	CORALIE	30
2018 May 15	SPECULOOS-Io	$I+z$
WASP-175		
2013 Jan–2014 June	WASP-South	86 025
2015 June–2018 July	CORALIE	20
2014 Apr 15	TRAPPIST-South	Blue blocking
2015 Dec 19	TRAPPIST-South	Blue blocking
2016 Dec 30	EulerCam	BG
2017 Feb 11	TRAPPIST-South	z'
WASP-182		
2006 May–2014 Nov	WASP-South	127 127
2016 June–2018 July	CORALIE	21
2018 Mar–2018 Nov	HARPS	14
2015 Oct 23	TRAPPIST-South	$I+z$
2018 June 28	Euler Cam	RG
2018 Aug 01	Euler Cam	RG
2018 Aug 11	TRAPPIST-South	$I+z$
2018 Aug 28	TRAPPIST-South	$I+z$

2.2 CORALIE spectroscopy

Several spectra at different epochs were obtained for all four targets using the high-resolution spectrograph CORALIE on the Swiss 1.2-m Euler telescope at La Silla Observatory, Chile (Queloz et al. 2001). CORALIE has a resolving power of $R \sim 60\,000$ and is fed by two fibres; one 2 arcsec on-sky science fibre encompassing the star and another that can either be connected to a Fabry–Pérot etalon for simultaneous wavelength calibration or on-sky for background subtraction of the sky flux. For WASP-169, WASP-171, and WASP-175 the CORALIE spectra were used to derive stellar parameters, see Section 3.1 for a detailed description of the analysis.

We obtained RVs for each epoch by cross-correlating with a binary G2 mask (Pepe et al. 2002). Bisector span, full width at half-maximum (FWHM), and other line-profile diagnostics were computed as well. Fig. 1 shows RVs and bisector span for the four stars, with Pearson coefficients. No correlation was found between the RVs and the bisector span. We also computed RVs using other binary masks ranging from A0 to M4, to check for any mask-dependent signal indicating a blend. As such, the CORALIE RVs confirm the planetary nature of the transit signals and we found them all to be in phase with the transit events detected by WASP-South.

Table 2 shows the first five RVs of WASP-169 from CORALIE, along with RV uncertainty, FWHM of the cross-correlation function (CCF), and bisector span. Full ASCII tables with all the RV data presented in this study are available online.

2.3 HARPS spectroscopy

To enable precise mass measurement of WASP-182b we also obtained HARPS RVs under programmes Anderson: 0100.C-0847 and Nielsen: 0102.C-0414 in 2018. HARPS is hosted by the ESO

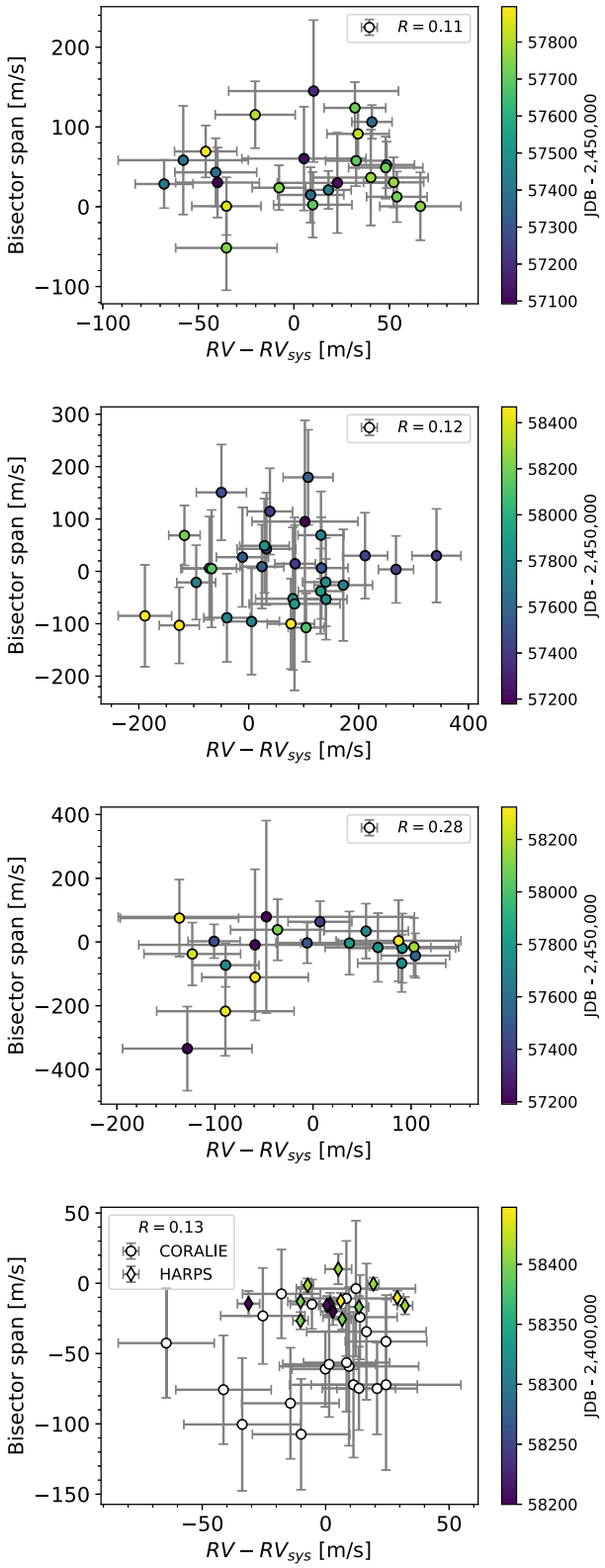

Figure 1. Bisector span and RVs for WASP-169, WASP-171, WASP-175, and WASP-182 from top to bottom panel. The Pearson coefficient R shows there is no correlation between the bisector span and RVs. For WASP-182 no offset in bisector span from CORALIE to HARPS was corrected for, and the Pearson coefficient is for the HARPS RVs only.

Table 2. The first five radial velocity (RV) measurements for WASP-169 from CORALIE, along with RV uncertainties, σ_{RV}, FWHM of the cross-correlation function (CCF), and bisector spans. BJD is Barycentric Julian Date. Full machine-readable tables for all four stars are available with the online journal.

Time (BJD – 240 0000)	RV (km s^{-1})	σ_{RV} (km s^{-1})	FWHM (km s^{-1})	Bisector (km s^{-1})
57092.695347	67.61532	0.02192	10.45130	0.03031
57119.639402	67.66054	0.03251	10.57522	0.06030
57121.569521	67.67801	0.03145	10.42107	0.02989
57185.451344	67.66557	0.04442	10.53662	0.14495
57365.775616	67.66402	0.01734	10.41273	0.01473
...	...	...	...	...

3.6-m telescope at La Silla Observatory, Chile (Mayor et al. 2003) and has a resolving power of $R \sim 100\,000$. The RVs were computed using the standard data reduction pipeline with a binary G2 mask, and confirmed the RV amplitude found with CORALIE, though with greater precision. The HARPS spectra were also used to derive spectral parameters for WASP-182, as detailed in Section 3.1.

2.4 EulerCam

Additional photometry was acquired for WASP-175 and WASP-182 using EulerCam (Lendl et al. 2012), also on the 1.2-m Swiss at La Silla Observatory. The observations used B and R filters, respectively. The data were bias and flat-field corrected and photometry extracted for a number of comparison stars and aperture radii. The comparison star ensemble and aperture radii chosen such that the scatter in a simple linear fit to the out of transit portion was minimized. The aim of this process was to produce a final light curve optimized to reduce the overall scatter.

2.5 TRAPPIST-North and -South

Both of the two 0.6-m TRAPPIST telescopes (Gillon et al. 2011; Jehin et al. 2011), based at La Silla and Oukaimeden Observatory in Morocco (Gillon et al. 2017; Barkaoui et al. 2019), were used to perform follow-up photometry on WASP-169, WASP-175, and WASP-182. All light curves of WASP-169 contain a meridian flip (MF), as detailed in Table 1. In the joint analysis of the RVs and photometry, described in Section 4, the data were partitioned at the time of MF and modelled as two independent data sets.

Data reduction consisted of standard calibration steps (bias, dark, and flat-field corrections) and subsequent aperture photometry using IRAF/DAOPHOT(Tody et al. 1986). Extraction of fluxes of selected stars using aperture photometry was performed with IRAF/DAOPHOT, as described in Gillon et al. (2013).

2.6 SPECULOOS-South

The robotic 1-m SPECULOOS Southern Observatory (SSO)-Io telescope is one of four telescopes at the SPECULOOS-South facility located at Paranal Observatory, Chile (Burdanov et al. 2018; Delrez et al. 2018; Gillon 2018; Jehin et al. 2018). It started its science operations in 2017 and observed one full transit of WASP-171 in 2018 May using an $I + z$ filter, toward the near-infrared end of the visible spectrum. The SPECULOOS telescopes are equipped with 2k × 2k CCD cameras, with increased sensitivities up to 1 μm, in the very-near-infrared. The calibration and photometric reduction of the data were performed as described in Gillon et al. (2013).

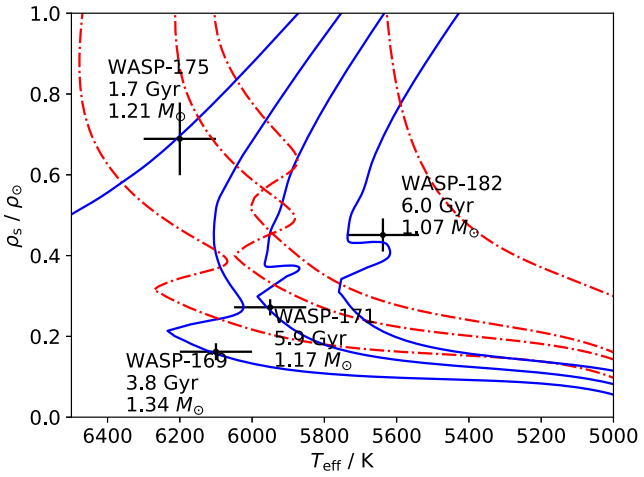

Figure 2. Isochrones (solid/blue) and evolution tracks (dot–dashed/red) output by BAGEMASS for each of the four host stars (labelled).

3 STELLAR PARAMETERS

3.1 Spectral characterization

Following the methods described in Doyle et al. (2013) we used the CORALIE and HARPS spectra to derive stellar parameters. Effective temperature, $T_{\rm eff}$, is computed from the Hα line. Surface gravity, $\log g$, is based on Na I D and Mg I b lines. The metallicity, [Fe/H], is determined from the equivalent width of a selection of unblended Fe lines. Lithium abundances that can be used to gauge stellar age and has been proposed to be a tracer of planet formation (King et al. 1997; Figueira et al. 2014) are derived as well. The uncertainty on $T_{\rm eff}$ and $\log g$ is propagated through to the abundances.

The projected rotational velocity, $V \sin i$, is found by convoluting the width of stellar absorption lines with the instrumental resolution ($R \sim 60\,000$ for CORALIE and $R \sim 100\,000$ for HARPS) and modelling macro turbulence by the method proposed in Doyle et al. (2014). Micro turbulence was estimated using the calibration from Bruntt et al. (2012).

3.2 Stellar masses and ages with BAGEMASS

We used the Bayesian stellar evolution code BAGEMASS (Maxted, Serenelli & Southworth 2015) to model stellar masses and ages based on spectral $T_{\rm eff}$ and [Fe/H] and the stellar density derived from the transit light curves. BAGEMASS samples a dense grid of stellar models to compute stellar masses and ages. The stellar masses obtained were used as Gaussian inputs in the final joint model. Fig. 2 shows the stellar evolutionary tracks and isochrones for all four planet host stars. All adopted stellar parameters from spectral characterization, BAGEMASS, and the final joint model are listed in Table 3.

3.3 Rotational modulation

We searched for rotational modulation caused by stellar spots in the WASP-South light curves for the four host stars using the method described in Maxted et al. (2011). Star-spots have limited lifetimes and will have variable distribution on the stellar surface over time. Therefore the modulation is not expected to be coherent, and so we searched each season of WASP-South data individually. WASP-169 and WASP-171 showed no significant modulation, with an upper limit on the amplitude of 1.5 mmag. For WASP-175 we can set an upper limit of 2 mmag.

For WASP-182 we find a possible modulation in the data from both 2009 and 2010, with a false-alarm probability of 1 per cent in each case. The modulation has a period of 30 $\pm$ 2 d and an amplitude of 1–2 mmag, which is near the detection limit in WASP-South data. In 2008 we saw a peak near (but not exactly at) half the period seen in 2009 and 2010, which could thus be the first harmonic of the rotational modulation (see Fig. 3). The exact position of the strongest peak in the data from 2009 and 2010 differs slightly. This could be a result of tracking star-spots at different latitudes on the stellar disc between the two seasons, which in the presence of differential rotation will cause a phase shift in modulation. Another possibility is star-spot groups coming and going during the season, which also will induce a period shift in the periodogram. In data both before (2006 and 2007) and after (2011 and 2012) these years, we see no significant modulation, though in each case the data are less extensive than in 2009 and 2010. The 30-d rotation period corresponds to a rotational velocity of about 2 km s^{-1} and is consistent with the $V \sin i$ computed from HARPS spectra (1.4 $\pm$ 1.0 km s^{-1}).

4 SYSTEM PARAMETERS

The full set of system parameters was modelled jointly using the discovery photometry, follow-up light curves, and RV data with the MCMC code described in detail in Collier Cameron et al. (2007) and Anderson et al. (2015). The analytic eclipse expressions derived by Mandel & Agol (2002) are used with a four-parameter, non-linear limb darkening law of Claret (2000, 2004). We have interpolated coefficients for stellar temperature and metallicity of each star, and in each photometric filter. The values used were perturbed during the MCMC via $T_{\rm L\text{-}D}$, the 'limb-darkening temperature', which has a mean and standard deviation corresponding to the spectroscopic $T_{\rm eff}$ and its uncertainty.

We ran the MCMC both with the eccentricity as a free parameter and fixed to zero, to check if the results are compatible with a circular orbit. We expect most giant planets in short-period orbits to have been circularized by tidal forces, and want to avoid overestimating the eccentricity in orbits that have none. Each circular model has six fitted parameters: orbital period, P, epoch, $T_{\rm C}$, transit depth in the absences of dark limb effects, $(R_{\rm p}/R_{\rm s})^2$, transit duration, T_{14}, impact parameters, b, and stellar RV semi-amplitude, K_1. The RV systemic velocity γ was fitted too, and in the case of WASP-171 along with a linear RV drift, $\dot{\gamma}$. For WASP-182, where we have data from two different spectrographs, an offset between CORALIE and HARPS was modelled as well.

For each target we ran 5000 MCMC steps as a 'burn in phase' to initialize the main phase that was set to have 50 000 iterations. At each step the free parameters are perturbed and the models are refit. If the χ^2 of the fit is better than the previous step, the current parameters are accepted, if the fit is worse, the parameters are accepted with a probability proportional to $\exp(-\Delta\chi^2)$. We used Gelman–Rubin statistics (Gelman et al. 2003; Ford 2006) to check how well the chains converge. In our case the Gelman–Rubin statistics indicated that all fitted parameters were well mixed.

Continuing our practice from recent discovery papers (e.g. Hellier et al. 2019) we treat the stellar parameters through a two-step process; we first estimate the stellar density, $\rho_{\rm s}$, from the transit duration alone, independently of stellar models. Secondly, we obtain stellar masses by using $\rho_{\rm s}$, $T_{\rm eff}$, and [Fe/H] in the stellar evolution model BAGEMASS, as explained in Section 3.2. The resulting stellar

Table 3. System parameters for WASP-169, WASP-171, WASP-175, and WASP-182, based on the analysis presented in Sections 3 and 4. Adopted non-SI units are $M_\odot = 1.9891 \times 10^{30}$ kg, $R_\odot = 6.95508 \times 10^8$ m, $R_{\rm Jup} = 7.149253763 \times 10^7$ m, and $M_{\rm Jup} = M_\odot/1047.52$.

Parameter	Symbol (Unit)	WASP-169	WASP-171	WASP-175	WASP-182
Stellar parameters					
WASP-South ID	1SWASP J...	082932.97−125640.9	112722.86−440519.3	110516.60−340720.3	204641.58−414915.2
2MASS ID[a]		J08293295−1256411	J11272283−4405193	J11051653−3407219	J20464156−4149151
Right ascension	RA (hh:mm:ss)	08:29:32.97	11:27:22.86	11:05:16.60	20:46:41.58
Declination	Dec. (dd:mm:ss)	−12:56:40.9	−44:05:19.3	−34:07:20.3	−41:49:15.2
Visual magnitude[b]	mV (mag)	12.17	13.05	12.04	11.98
Stellar mass	$M_{\rm s}$ ($M_\odot$)	1.337 ± 0.083	1.171 ± 0.058	1.212 ± 0.045	1.076 ± 0.064
Stellar radius	$R_{\rm s}$ ($R_\odot$)	$2.011^{+0.188}_{-0.089}$	$1.637^{+0.091}_{-0.046}$	1.204 ± 0.064	1.34 ± 0.03
Effective temp.[c]	$T_{\rm eff}$ (K)	6110 ± 101	5965 ± 100	6229 ± 100	5638 ± 100
Stellar metallicity[c]	[Fe/H]	0.06 ± 0.07	0.04 ± 0.07	0.150 ± 0.069	0.27 ± 0.11
Lithium abundance[c]	log A (Li)	None found	$\sim 1.1 \pm 0.2$	2.16 ± 0.08	2.0 ± 0.09
Macro-turbulent vel.[d]	$V_{\rm mac}$ (km s^{-1})	5.0	4.4	≤ 4.8	3.4 ± 0.7
Projected rot. vel.[e]	$V \sin i$ (km s^{-1})	4.3 ± 0.9	6.3 ± 0.9	≤ 4.0	1.4 ± 1.0
Age[f]	(Gyr)	3.802 ± 0.779	5.908 ± 1.051	1.745 ± 0.995	5.952 ± 2.684
Distance[g]	d (pc)	638 ± 14	774 ± 20	584 ± 13	331 ± 4.6
Stellar density	$\rho_{\rm s}$ ($\rho_\odot$)	$0.166^{+0.019}_{-0.039}$	$0.270^{+0.017}_{-0.042}$	$0.693^{+0.125}_{-0.094}$	0.451 ± 0.041
Surface gravity	log ($g_{\rm s}$) (cgs)	$3.958^{+0.033}_{-0.076}$	$4.080^{+0.020}_{-0.049}$	4.359 ± 0.045	4.218 ± 0.033
Planet parameters					
Planet mass	$M_{\rm p}$ ($M_{\rm Jup}$)	0.561 ± 0.061	1.084 ± 0.094	0.99 ± 0.13	0.148 ± 0.011
Planet radius	$R_{\rm p}$ ($R_{\rm Jup}$)	$1.304^{+0.150}_{-0.073}$	$0.98^{+0.07}_{-0.04}$	1.208 ± 0.081	0.850 ± 0.030
Period	P (d)	5.6114118 ± 0.0000092	3.8186244 ± 0.0000038	$3.0652907^{+0.0000011}_{-0.0000016}$	3.3769848 ± 0.0000024
Transit epoch	$T_{\rm C} - 240\,0000$	57697.0176 ± 0.0014	58059.8295 ± 0.0011	57143.78886 ± 0.00034	58018.66018 ± 0.00067
Transit duration	T_{14} (d)	$0.2522^{+0.0042}_{-0.0034}$	0.1908 ± 0.0024	0.1115 ± 0.0017	0.1082 ± 0.0015
Transit depth	$(R_{\rm p}/R_{\rm s})^2$	0.00446 ± 0.00028	0.00382 ± 0.00018	0.01064 ± 0.00036	0.00426 ± 0.00017
Scaled semimajor axis	$a/R_{\rm s}$	$7.30^{+0.68}_{-0.26}$	$6.64^{+0.38}_{-0.13}$	7.86 ± 0.41	$8.3^{+1.9}_{-1.4}$
Semimajor axis	a (au)	0.0681 ± 0.0014	0.05040 ± 0.00083	0.04403 ± 0.00055	0.0451 ± 0.0009
Impact parameter	b	0.27 ± 0.19	$0.19^{+0.19}_{-0.13}$	$0.640^{+0.043}_{-0.061}$	0.775 ± 0.019
Orbital eccentricity	e	0 (adopted, $2\sigma < 0.17$)	0 (adopted, $2\sigma < 0.16$)	0 (adopted, $2\sigma < 0.28$)	0 (adopted, $2\sigma < 0.25$)
Orbital inclination	i (°)	$87.9^{+1.4}_{-2.0}$	$88.3^{+1.1}_{-1.9}$	85.33 ± 0.62	83.88 ± 0.33
RV semi-amplitude	K_1 (m s^{-1})	52.9 ± 5.4	126 ± 10	124 ± 17	19.0 ± 1.2
Systemic RV	γ (km s^{-1})	67.6553 ± 0.0035	10.4838 ± 0.0078	5.38 ± 0.01	-34.1325 ± 0.0038[h]
RV drift	$\dot{\gamma}$ (km s^{-1} yr^{-1})	–	-0.07659 ± 0.0085	–	–
RV residuals	σ(res$_{\rm RV}$) (m s^{-1})	18	34	6.5[i]	34
Reduced RV fit χ^2	$\chi^2_{\rm r}$	1.2	1.1	1.9	0.43
Planet density	ρ_p ($\rho_{\rm Jup}$)	$0.249^{+0.056}_{-0.071}$	$1.13^{+0.17}_{-0.22}$	$0.56^{+0.15}_{-0.11}$	0.240 ± 0.044
Surface gravity	log ($g_{\rm p}$) (cgs)	$2.87^{+0.07}_{-0.10}$	$3.405^{+0.049}_{-0.069}$	3.194 ± 0.077	2.669 ± 0.049
Equilibrium temperature	$T_{\rm eq}$ (K)	1604^{+74}_{-42}	1642^{+51}_{-35}	1571 ± 49	1479 ± 34

[a] Cutri et al. (2003).
[b] From NOMAD (Zacharias et al. 2004).
[c] From spectral analysis of CORALIE spectra (HARPS for WASP-182 (Section 3.1).
[d] Derived via the method by Doyle et al. (2014) on CORALIE and HARPS spectra.
[e] Derived from CORALIE and HARPS spectra, assuming macroturbulent velocity.
[f] From BAGEMASS analysis (Section 3.2).
[g] From *Gaia* Data Release 2 (DR2) parallax (Gaia Collaboration et al. 2016, 2018a).
[h] RV offset of 31.9 ± 0.2 m s^{-1} from CORALIE to HARPS is found.
[i] RV residual for HARPS and CORALIE combined.

mass estimate and its uncertainty are finally used as input in the MCMC to derive stellar radii. The stellar density for WASP-182 is poorly constrained by the transit data alone, so we used an additional prior on the radius from *Gaia* Data Release 2 (DR2), as described in Turner et al. (2019).

5 RESULTS

For each system we list the final stellar and planetary parameters in Table 3 with 1σ errors. Figs 4–8 show the final joint model fitted to the discovery and follow-up data.

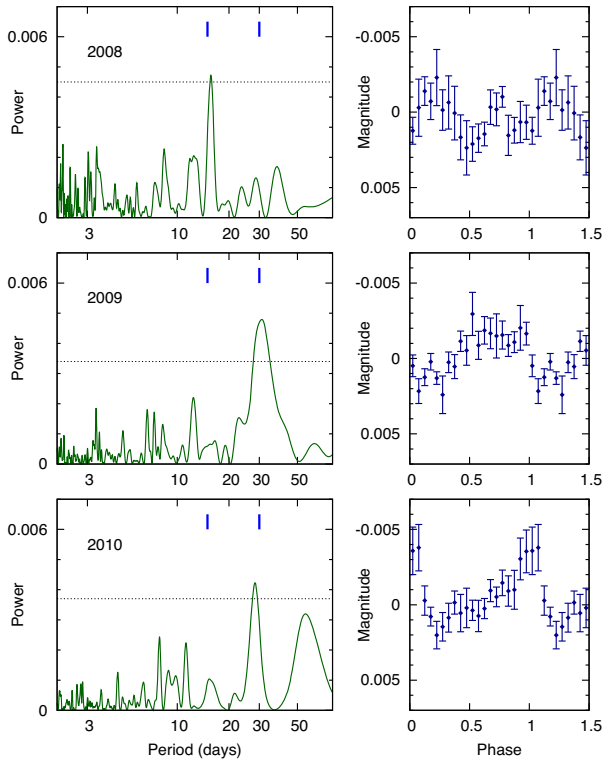

Figure 3. Periodograms of the WASP-South data for WASP-182 from three different years (left) along with folds of the data at the possible rotational periods (right). The folded data have been binned to 20 bins, each corresponding to 1.5 nights. The blue marks are at 30 and 15 d and the dotted horizontal line at 1 per cent false alarm probability (FAP).

5.1 WASP-169b

WASP-169b is a low-density Jupiter with mass $0.561 \pm 0.061\ M_{\rm Jup}$ and radius $1.304^{+0.150}_{-0.073}\ R_{\rm Jup}$ in a 5.611 d orbit around a $V = 12.17$ F8 subgiant. Fig. 4 shows the WASP-South discovery light curve with follow-up observations from TRAPPIST-North, -South, and CORALIE. The planetary and stellar parameters are well constrained. The transit $\log(g_{\rm s}) = 3.958^{+0.033}_{-0.076}$ (cgs) is consistent with the spectroscopic value of 4.0 ± 0.2. The resulting stellar radius ($2.011^{+0.188}_{-0.089}\ {\rm R}_\odot$) is in agreement with *Gaia* DR2 ($2.28^{+0.10}_{-0.25}\ {\rm R}_\odot$). WASP-169 has a faint star 7 arcsec away with $\Delta g = 5.4$ (Gaia Collaboration et al. 2018a). It has a similar parallax (1.26 ± 0.09 mas versus 1.566 ± 0.04 mas), but does not appear to be comoving.

The low density of WASP-169b ($0.249^{+0.056}_{-0.071}\ \rho_{\rm jup}$) should make it a good candidate for atmospheric characterization. It has an estimated scale height of 1300 km, corresponding to a transmission signal of 121 ppm. The *James Webb Space Telescope* (*JWST*) instrument NIRSpec will uniquely be able to cover the near-infrared spectral range from 0.6 to 5.3 μm in one low-resolution spectrum in 'PRISM mode' (Birkmann et al. 2016). With a *J*-band magnitude of 10.8, WASP-169 is a perfect target for NIRSpec, expecting to achieve signal-to-noise ratio, SNR, 10 000–25 000 per resolution element across the spectrum with one transit (Nielsen et al. 2016; Batalha et al. 2017).

5.2 WASP-171b

WASP-171 is a $V = 13.05$ G0 star that also appears to be slightly evolved. The transit $\log(g_{\rm s}) = 4.080^{+0.020}_{-0.049}$ (cgs) is consistent with

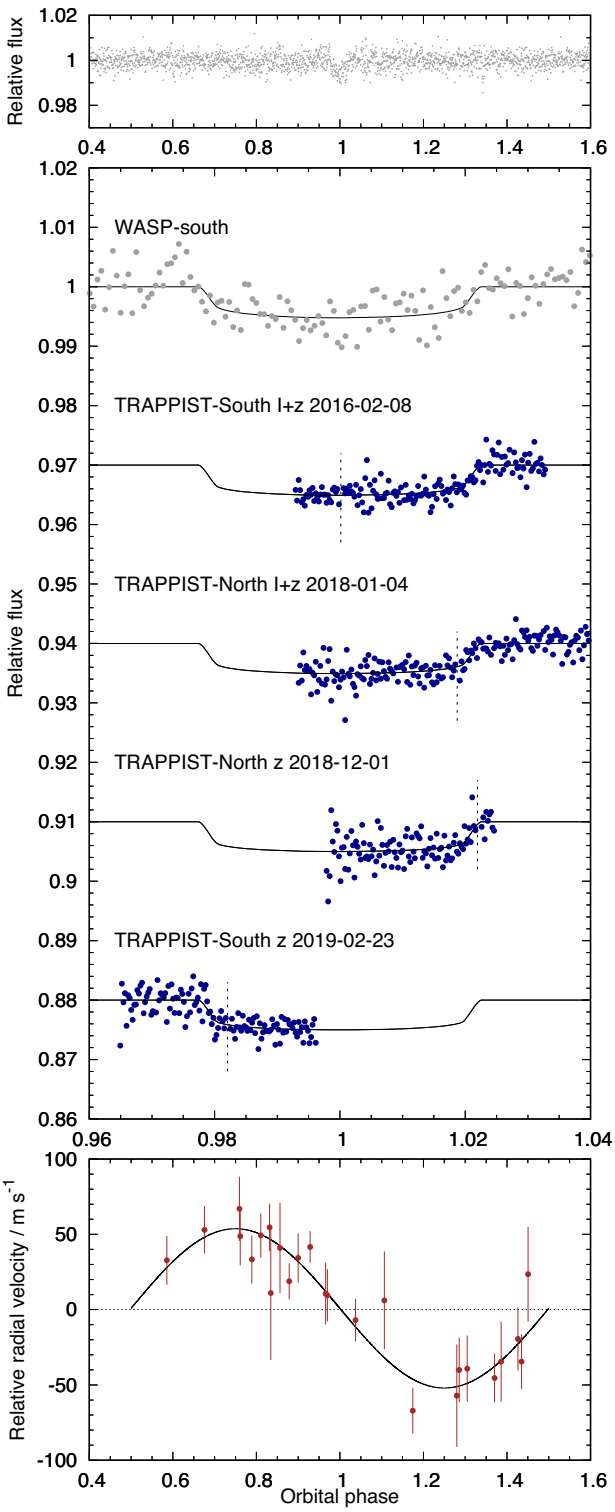

Figure 4. Data for the WASP-169 system. Top: WASP discovery light curve phase folded on period found by joint analysis and binned to 2 min. Middle: light curves used in joint analysis. The WASP light curve has been binned to 5 min and is shown as grey points with the transit model overplotted. The follow-up light curves have been binned to 2 min and are here all from TRAPPIST-North and -South shown in blue. Times of meridian flip are indicated as vertical dashed lines. Bottom: CORALIE radial velocities used in the joint analysis overplotted with resulting model.

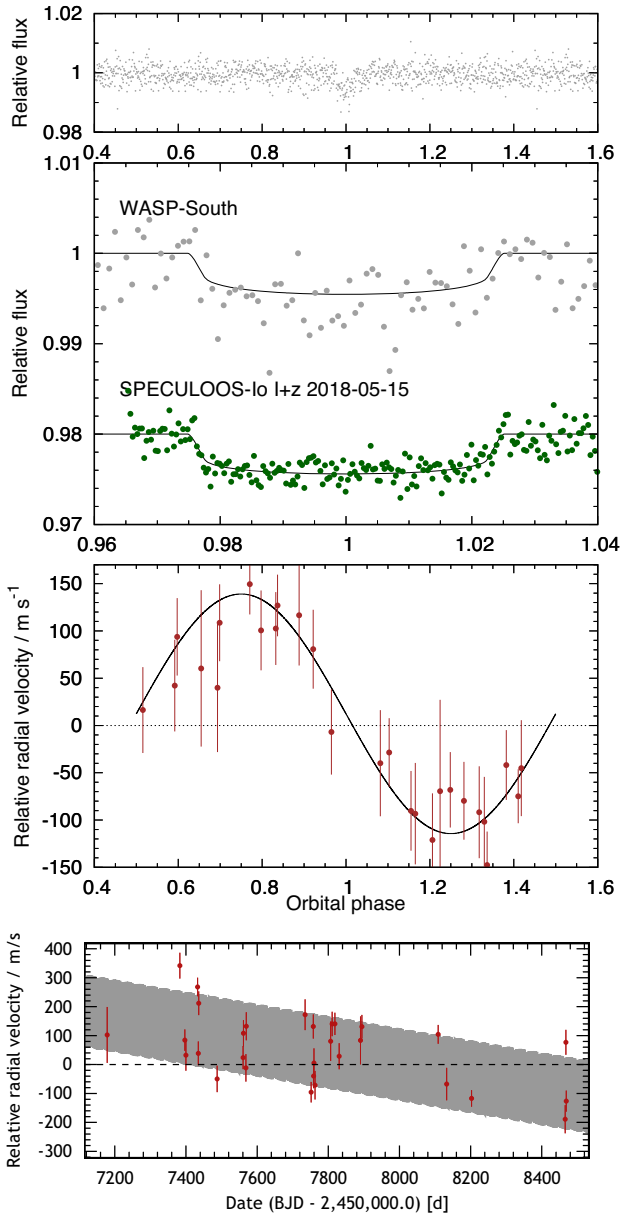

Figure 5. Same as Fig. 4, but for the WASP-171 system with the RV time series added in the bottom panel. The best-fitting Keplerian model is overplotted with the adopted linear trend. Data from SPECULOOS are shown in green in the second panel from the top.

the spectroscopic value of 4.1 ± 0.2. We do find a slight discrepancy between our radius estimate ($1.637^{+0.091}_{-0.046}\,R_\odot$) and the *Gaia* DR2 value ($2.11^{+0.04}_{-0.2}\,R_\odot$), though they are consistent to 2σ. The *Gaia* measurements do not seem to be affected by any excess astrometric or photometric noise.

WASP-171b is found to have a mass of $1.0841 \pm 0.094\,M_{\rm Jup}$ and radius $0.98^{+0.07}_{-0.04}\,R_{\rm Jup}$, fitting the characteristics of a fairly typical hot Jupiter. The orbital period is 3.82 d, making it the hottest planet presented in this paper with an equilibrium temperature of $T_{\rm eq} = 1640 \pm 40$ K. Fig. 5 shows the WASP-South discovery light curve with follow-up observations from SPECULOOS-Io and CORALIE. The RVs span a baseline of 3.6 yr and show a linear drift of 77 ± 9 m s^{-1} yr^{-1}, indicating a third body further out in the system. With the data available we can put a minimum mass limit of 10 $M_{\rm Jup}$ on the outer object, though more observations are needed to constrain whether it is substellar or not.

5.3 WASP-175b

WASP-175 is a $V = 12.04$ F7 star with metallicity [Fe/H] $= 0.150 \pm 0.069$. The transit $\log(g_{\rm s}) = 4.359 \pm 0.045$ (cgs) is consistent with the spectroscopic value of 4.3 ± 0.2.

Fig. 6 shows the WASP-South discovery light curve with follow-up observations from TRAPPIST-South, EulerCam, and CORALIE. The WASP-South light curve is diluted by a star 7.9 arcsec away with $\Delta g = 1.5$ (Gaia Collaboration et al. 2018a). The fitted depth of the transit is driven by the follow-up photometry in which the two stars are spatially resolved. The neighbouring star has similar *Gaia* DR2 parallax and is comoving with WASP-175, indicating that the two stars might be in a wide S-type binary orbit. The projected separation of the two stars is 4600 au. Fig. 7 shows the two stars with their common proper motion indicated as pink arrows, WASP-175 is the star in the centre of the image. There are two other faint *Gaia* sources in the field that do not share the same parallax. The companion to the north has *Gaia* radius $0.88 \pm 0.10\,R_\odot$ and effective temperature 5163^{+491}_{-165} K.

WASP-175b has mass $0.99 \pm 0.13\,M_{\rm Jup}$, radius $1.208 \pm 0.081\,R_{\rm Jup}$, and orbits every 3.07 d at a distance of 0.044 au. Much like the first discovery of a transiting exoplanet (HD 209458b; Charbonneau et al. 2000) and many more since then, WASP175b falls in the category of hot Jupiters showing anomalous large radii, which cannot be explained by a H–He-dominated planet interior (Baraffe, Chabrier & Barman 2009). The low density of the planet ($0.56^{+0.15}_{-0.11}\rho_{\rm jup}$) should make WASP-175b a good candidate for atmospheric characterization. It has an estimated scale height of 620 km, corresponding to a transmission signal of 150 ppm.

5.4 WASP-182b

WASP-182 is a $V = 11.98$ G5 star with a high metallicity, [Fe/H] $= 0.27 \pm 0.11$. The stellar density was poorly constrained by the available photometric data, and we thus enforced a prior on the stellar radius from *Gaia* DR2 in the MCMC modelling. The resulting stellar surface gravity $\log(g_{\rm s}) = 4.218 \pm 0.033$ (cgs) is consistent with the spectroscopic value of 4.2 ± 0.2.

Fig. 8 shows the WASP-South discovery light curve with follow-up observations from TRAPPIST-South, EulerCam, CORALIE, and HARPS. With a RV semi-amplitude of 19.0 ± 1.2 m s^{-1} a larger telescope was needed to precisely measure the mass of WASP-128b, and we thus obtained data with HARPS as well. The RV scatter around the best-fitting model is 6.5 m s^{-1}. One point close to phase = 0 (though not in-transit) shows a relatively large offset (7 m s^{-1}) from the joint fit. It does not appear to be affected by stellar activity or other systematic effects, so we have included it in the analysis for completion. Using the WASP-South photometry we constrain the stellar rotation period to 30 ± 2 d, which is consistent with a G star on the main sequence (McQuillan, Mazeh & Aigrain 2014). The RVs show no variability, as a sign of stellar activity, at that period.

WASP-182b is found to have a mass of $0.148 \pm 0.011\,M_{\rm Jup}$ and radius $0.850 \pm 0.030\,R_{\rm Jup}$, making it a low-density planet. The estimated scale height is 1930 km, corresponding to 264 ppm. With a period of 3.38 d WASP-182b sits right between the lower and upper edges of the sub-Jovian desert in both the mass and radius plane, as seen in Fig. 9. This makes it an even more compelling target for in-depth atmospheric characterization, studying possible atmospheric escape close to the evaporation desert (Ehrenreich et al. 2015; Bourrier et al. 2018; Owen 2019).

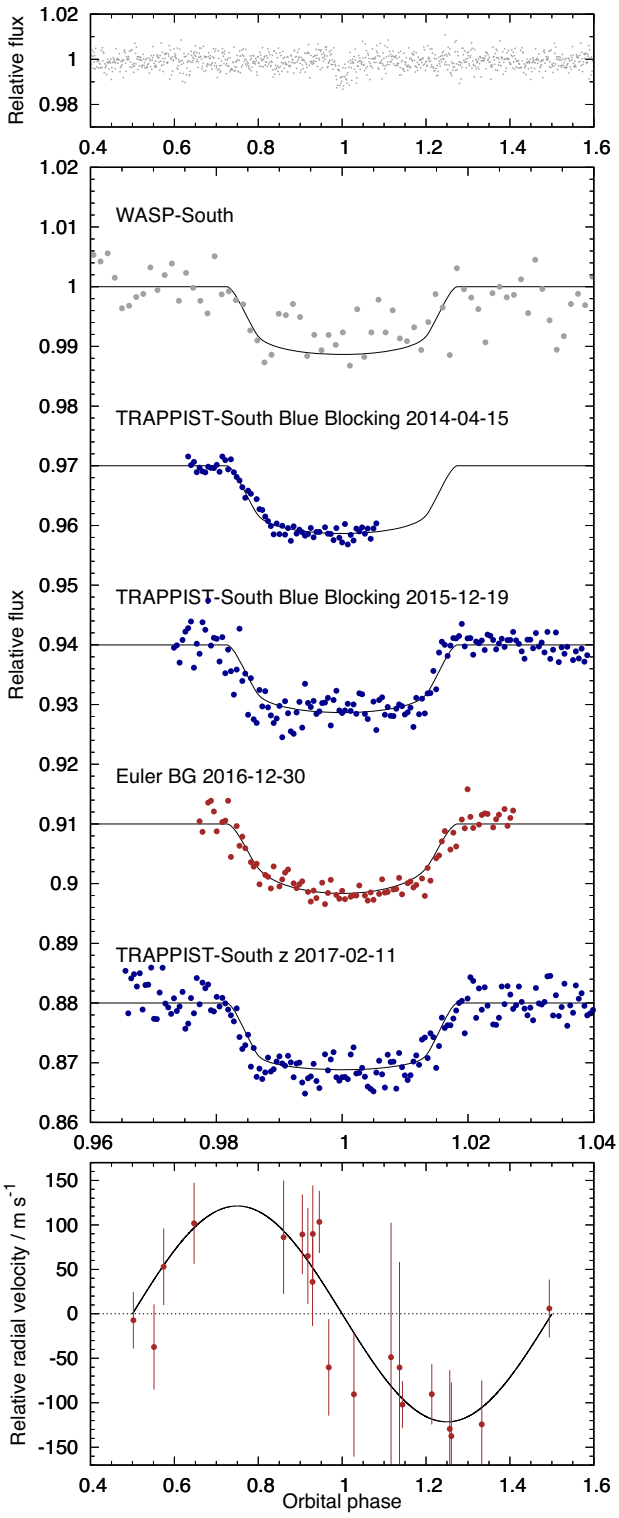

Figure 6. Same as Fig. 4, but for the WASP-175 system. Data from EulerCam are shown in red in the middle panel.

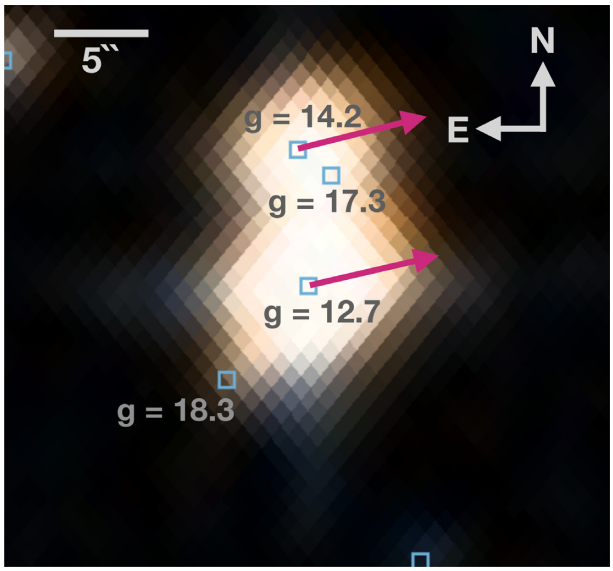

Figure 7. DSS image of WASP-175 (centre) and the nearby companion 7.9 arcsec north. Their common proper motions are indicated as pink arrows. Blue squares are *Gaia* DR2 sources in the field, with *Gaia* magnitudes denoted in grey.

6 DISCUSSION AND CONCLUSION

We have presented the discovery and mass determination of four new Jovian planets from the WASP-South survey. Fig. 9 presents these planets along with the mass and radii of the known exoplanet population, as per 2019 March. Only planets with masses determined to a fractional accuracy of 20 per cent or better are included, and mass estimates based on transit-timing variations (TTVs) are distinguished in grey.

WASP-169b, WASP-171b, and WASP-175b fall within the category of hot Jupiters, with WASP-169b and WASP-175b being inflated. Having precise parameters for inflated Jupiters across a variety of stellar hosts and evolutionary stages will help to solve the conundrum of the hot Jupiter radius anomaly.

WASP-182b is a bloated sub-Saturn mass planet, occupying a poorly populated parameter space, corresponding to the transition between Neptune-like ice giants and Saturn-like gas giants, at 0.05–0.3 $M_{\rm Jup}$. Less than 30 planets in this range have masses determined to 20 per cent fractional accuracy or better.

Furthermore, WASP-182b sits right in the apex of the sub-Jovian desert, as defined by Mazeh et al. (2016) and Szabó & Kiss (2011), see Fig. 10. The proposed mechanisms behind this dearth of sub-Saturn planets with short periods are numerous, but can generally be classified as being related to disc material available during planet formation or photoevaporation for the small planets. For the larger ones, framing the top of the desert, migration of massive planet from further out in the system could allow the most massive objects to keep their atmospheric volatile layer as they approach the host star (Lopez & Fortney 2014; Mordasini et al. 2015). Whereas less massive planets will lose their outer layer and perhaps end up as a naked core in the bottom of the desert (Owen & Lai 2018). Finding planets such as WASP-182b that sits between the two edges will help to identify the most important physical processes behind the desert.

ACKNOWLEDGEMENTS

We thank the Swiss National Science Foundation (SNSF) and the Geneva University for their continuous support to our planet search programs. This work has been in particular carried out in the frame of the National Centre for Competence in Research 'PlanetS' supported by the Swiss National Science Foundation (SNSF).

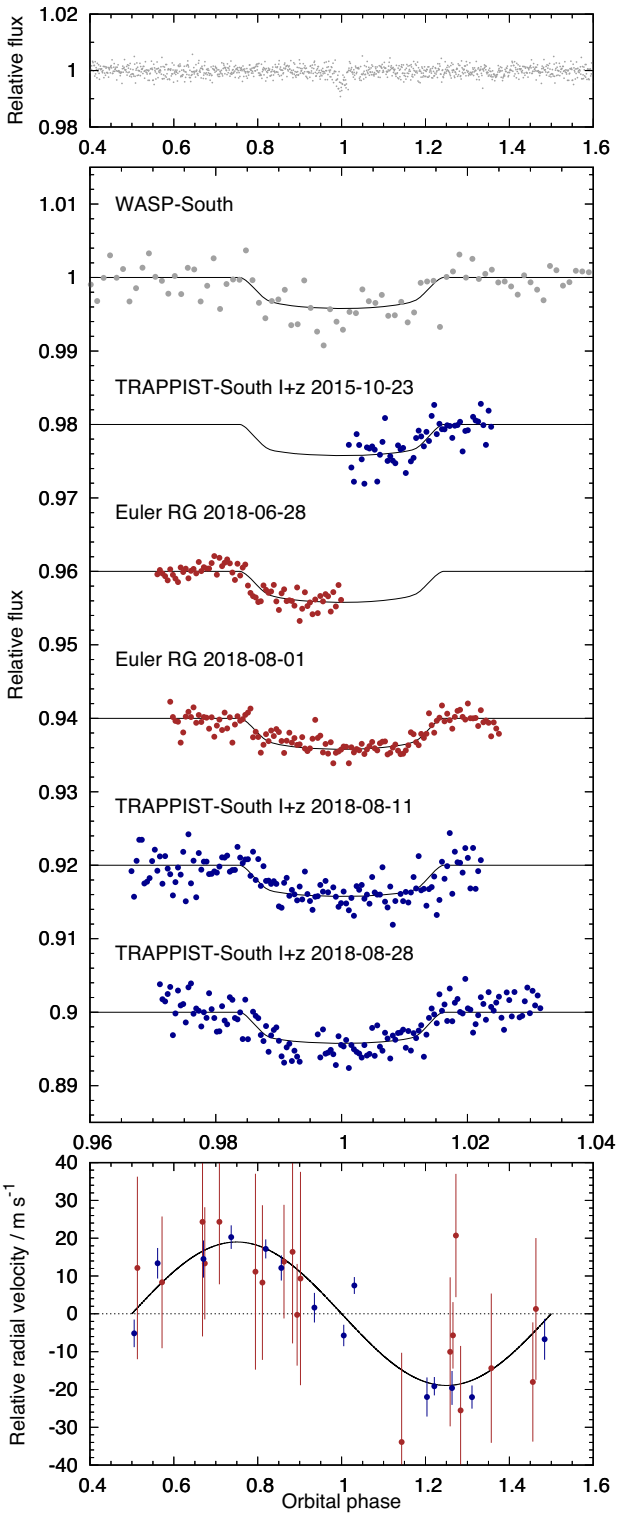

Figure 8. Same as Fig. 6, but for the WASP-182 system. Data from HARPS are shown in blue in the bottom panel.

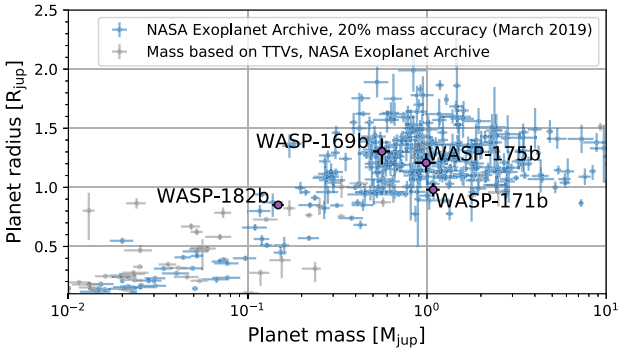

Figure 9. Masses and radii of the four planets presented in this paper: WASP-169b, WASP-171b, WASP-175b, and WASP-182b, along with the known exoplanet population. Only planets with masses determined to 20 per cent or better are included, and mass estimates based on transit-timing variations (TTVs) are in grey.

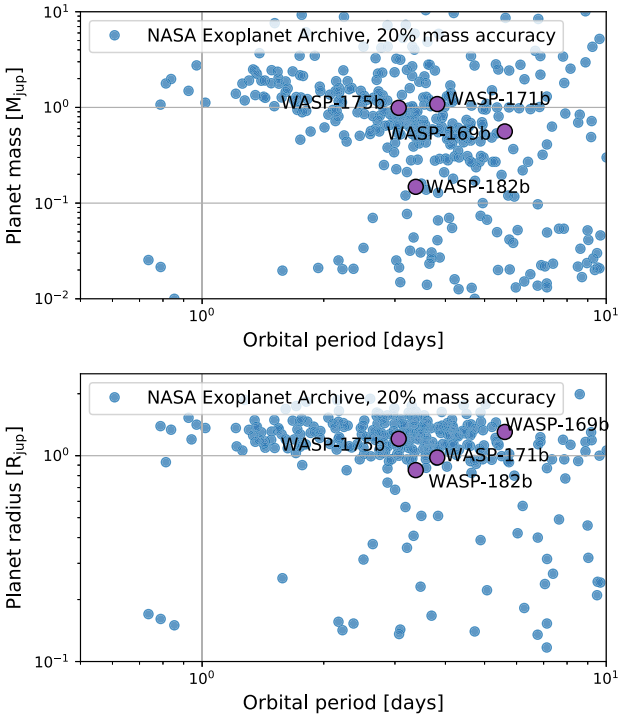

Figure 10. The sub-Jovian deserts illustrated through the know exoplanet population with masses determined to 20 per cent or better, as in Fig. 9. Top panel shows the mass–period plane, whereas the bottom panel shows the same dearth of sub-Jovian planets with short periods in the radius–period plane. WASP-182b sits at the apex of the sub-Jovian desert in both the mass and radius planes.

This publication makes use of The Data and Analysis Center for Exoplanets (DACE), which is a facility based at the University of Geneva (CH) dedicated to extrasolar planets data visualization, exchange, and analysis. DACE is a platform of the Swiss National Centre of Competence in Research (NCCR) PlanetS, federating the Swiss expertise in Exoplanet research. The DACE platform is available at https://dace.unige.ch.

WASP-South is hosted by the South African Astronomical Observatory and we are grateful for their ongoing support and assistance. Funding for WASP comes from consortium universities and from the UK's Science and Technology Facilities Council. TRAPPIST is funded by the Belgian Fund for Scientific Research (Fond National de la Recherche Scientifique, FNRS) under the grant FRFC 2.5.594.09.F, with the participation of the Swiss National Science Foundation (SNF). MG and EJ are FRS – FNRS Senior Research Associates.

The research leading to these results has received funding from the European Research Council under the FP/2007-2013 ERC Grant Agreement 336480, from the ARC grant for Concerted Research Actions financed by the Wallonia-Brussels Federation, from the Balzan Foundation, and a grant from the Erasmus + International Credit Mobility programme (KB).

REFERENCES

Anderson D. R. et al., 2015, A&A, 575, A61
Anderson D. R. et al., 2018, preprint (arXiv:1809.04897)
Baraffe I., Chabrier G., Barman T., 2009, Rep. Progress Phys., 73, 016901
Barkaoui K. et al., 2019, AJ, 157, 43
Batalha N. E. et al., 2017, PASP, 129, 064501
Birkby J. L., de Kok R. J., Brogi M., de Mooij E. J. W., Schwarz H., Albrecht S., Snellen I. A. G., 2013, MNRAS, 436, L35
Birkmann S. M. et al., 2016, Proc. SPIE, 9904, 99040B
Borucki W. J. et al., 2010, Science, 327, 977
Bourrier V. et al., 2018, A&A, 620, A147
Brogi M., de Kok R. J., Albrecht S., Snellen I. A. G., Birkby J. L., Schwarz H., 2016, ApJ, 817, 106
Bruntt H. et al., 2012, MNRAS, 423, 122
Burdanov A., Delrez L., Gillon M., Jehin E., 2018, in Deeg H., Belmonte J., eds, Handbook of Exoplanets. Springer, Cham, Switzerland, p. 1007
Charbonneau D., Brown T. M., Latham D. W., Mayor M., 2000, ApJ, 529, L45
Claret A., 2000, A&A, 363, 1081
Claret A., 2004, A&A, 428, 1001
Collier Cameron A. et al., 2006, MNRAS, 373, 799
Collier Cameron A. et al., 2007, MNRAS, 380, 1230
Skrutskie M. F. et al., 2006, The Two Micron All Sky Survey (2MASS), AJ, 131, 1163
de Kok R. J., Brogi M., Snellen I. A. G., Birkby J., Albrecht S., de Mooij E. J. W., 2013, A&A, 554, A82
Delrez L. et al., 2018, Proc. SPIE, 10700, 107001I
Doyle A. P. et al., 2013, MNRAS, 428, 3164
Doyle A. P., Davies G. R., Smalley B., Chaplin W. J., Elsworth Y., 2014, MNRAS, 444, 3592
Ehrenreich D. et al., 2015, Nature, 522, 459
Figueira P., Faria J. P., Delgado-Mena E., Adibekyan V. Z., Sousa S. G., Santos N. C., Israelian G., 2014, A&A, 570, A21
Ford E. B., 2006, ApJ, 642, 505
Fulton B. J., Petigura E. A., 2018, AJ, 156, 264
Gaia Collaboration et al., 2016, A&A, 595, A1
Gaia Collaboration et al., 2018a, A&A, 616, A1
Gelman A., Carlin J. B., Stern H. S., Rubin D. B., 2003, Bayesian Data Analysis, 2nd edn. Chapman & Hall/CRC, London
Gillon M., 2018, Nat. Astron., 2, 344
Gillon M. et al., 2011, A&A, 533, A88
Gillon M., Jehin E., Delrez L., Magain P., Opitom C., Sohy S., 2013, Protostars and Planets VI Posters, Heidelberg, 15–20 July 2013
Gillon M. et al., 2017, Nature, 542, 456
Hellier C. et al., 2019, MNRAS, 482, 1379
Jehin E. et al., 2011, The Messenger, 145, 2
Jehin E. et al., 2018, The Messenger, 174, 2
King J. R., Deliyannis C. P., Hiltgen D. D., Stephens A., Cunha K., Boesgaard A. M., 1997, AJ, 113, 1871
Lendl M. et al., 2012, A&A, 544, A72
Lopez E. D., Fortney J. J., 2014, ApJ, 792, 1
McQuillan A., Mazeh T., Aigrain S., 2014, ApJS, 211, 24
Mandel K., Agol E., 2002, ApJ, 580, L171
Maxted P. F. L. et al., 2011, PASP, 123, 547
Maxted P. F. L., Serenelli A. M., Southworth J., 2015, A&A, 575, A36
Mayor M. et al., 2003, The Messenger, 114, 20
Mazeh T., Holczer T., Faigler S., 2016, A&A, 589, A75
Mordasini C., Molliére P., Dittkrist K. M., Jin S., Alibert Y., 2015, Int. J. Astrobiol., 14, 201
Nielsen L. D. et al., 2016, Proc. SPIE, 9904, 99043O
Owen J. E., 2019, Annu. Rev. Earth Planet. Sci., 47, 67
Owen J. E., Lai D., 2018, MNRAS, 479, 5012
Pepe F. et al., 2002, The Messenger, 110, 9
Pollacco D. L. et al., 2006, PASP, 118, 1407
Queloz D. et al., 2001, The Messenger, 105, 1
Ricker G. R. et al., 2015, J. Astron. Telesc. Instrum. Syst., 1, 014003
Snellen I. A. G., de Kok R. J., de Mooij E. J. W., Albrecht S., 2010, Nature, 465, 1049
Szabó G. M., Kiss L. L., 2011, ApJ, 727, L44
Tody D., 1986, in Crawford D. L., ed., Proc. SPIE Vol. 627, Instrumentation in Astronomy VI. SPIE, Bellingham, WA, p. 733
Turner O. D. et al., 2019, MNRAS , Three hot-Jupiter on the upper edge of the mass-radius distribution: WASP-177, WASP-181 and WASP-183, 485(4), 5790
West R. G. et al., 2019, MNRAS, 486, 5094
Zacharias N., Monet D. G., Levine S. E., Urban S. E., Gaume R., Wycoff G. L., 2004, BAAS, 36, 1418

SUPPORTING INFORMATION

Supplementary data are available at *MNRAS* online.
Please note: Oxford University Press is not responsible for the content or functionality of any supporting materials supplied by the authors. Any queries (other than missing material) should be directed to the corresponding author for the article.

[1]*Observatoire de Genève, Université de Genève, 51 Chemin des Maillettes, CH-1290 Sauverny, Switzerland*
[2]*Astrophysics Group, Keele University, Staffordshire ST5 5BG, UK*
[3]*Space Sciences, Technologies and Astrophysics Research (STAR) Institute, Université de Liège, 4031 Liège, Belgium*
[4]*Oukaimeden Observatory, High Energy Physics and Astrophysics Laboratory, Cadi Ayyad University, Marrakech, Morocco*
[5]*SUPA, School of Physics and Astronomy, University of St Andrews, North Haugh, Fife KY16 9SS, UK*
[6]*Cavendish Laboratory, J J Thomson Avenue, Cambridge CB3 0HE, UK*
[7]*Space Research Institute, Austrian Academy of Sciences, Schmiedlstr. 6, A-8042 Graz, Austria*
[8]*Department of Physics, University of Warwick, Coventry CV4 7AL, UK*
[9]*Centre for Exoplanets and Habitability, University of Warwick, Gibbet Hill Road, Coventry CV4 7AL, UK*
[10]*School of Physics and Astronomy, University of Birmingham, Edgbaston, Birmingham B15 2TT, UK*

This paper has been typeset from a TEX/LATEX file prepared by the author.